Frustrated pyrochlore oxides, $Y_2Mn_2O_7$, $Ho_2Mn_2O_7$, and $Yb_2Mn_2O_7$: Bulk magnetism and magnetic microstructure

J. E. Greedan and N. P. Raju
Brockhouse Institute for Materials Research, McMaster University, Hamilton, Ontario, Canada L8S 4M1

A. Maignan and Ch. Simon
Laboratoire CRISMAT, CNRS URA 1318, ISMRa, Université de Caen, Bd du Maréchal Juin, 14050 Caen Cédex, France

J. S. Pedersen
Department of Solid State Physics, Risø National Laboratory, DK-4000 Roskilde, Denmark

A. M. Niraimathi and E. Gmelin
Max-Planck Institut für Festköperforschung, Heisenbergstraβe 1, 70569 Stuttgart, Germany

M. A. Subramanian
Central Research and Development, E. I. DuPont de Nemours and Co., Wilmington, Delaware 19880-0328
(Received 21 February 1996)

The bulk magnetic properties, including dc and ac susceptibilities and heat capacity, of the pyrochlore oxides $Ho_2Mn_2O_7$ and $Yb_2Mn_2O_7$ are reported and compared with those of the previously studied $Y_2Mn_2O_7$. In the latter case the magnetic Mn^{4+} ions occupy the 16*c* sites in $Fd3m$ which define a potentially frustrated three-dimensional array of corner sharing tetrahedra. For $Ho_2Mn_2O_7$ and $Yb_2Mn_2O_7$ magnetic rare earth ions occupy the 16*d* sites, as shown by powder neutron diffraction, which are topologically equivalent to the 16*c* sites but displaced by a vector (1/2 1/2 1/2). $Ho_2Mn_2O_7$ and $Yb_2Mn_2O_7$ display sharp increases in both dc and ac susceptibilities near 38 K. In addition field-cooled-zero-field-cooled irreversibilities appear, also at 38 K, followed by broad maxima centered near 30 K. The ac data are similar with frequency variability setting below 38 K and broad, frequency dependent maxima at somewhat lower temperatures. Heat capacity data show only broad maxima centered near 30–35 K with a high temperature tail extending up to 80 K. The bulk behavior of $Ho_2Mn_2O_7$ and $Yb_2Mn_2O_7$ just described parallels the spin-glass-like behavior of $Y_2Mn_2O_7$ but with a doubling of the temperature scale. Surprisingly, neutron diffraction data for both $Ho_2Mn_2O_7$ and $Yb_2Mn_2O_7$ show resolution limited reflections of magnetic origin in contrast to the heat capacity results. The resolution of the neutron diffraction data places a minimum on the correlation length of 100 Å. Small angle neutron scattering data for all three materials are reported for the Q range 10^{-2} Å^{-1} to 2×10^{-1} Å^{-1} and the temperature range 6–100 K. Data for the full Q range can be fitted for all three materials to a model consisting of a Lorentzian and a Lorentzian-squared term, i.e., $I(Q)=A/(Q^2+1/\xi_1^2)+B/(Q^2+1/\xi_2^2)^2$, a cross section commonly found in spin-glass-like materials. A surprising result is that the correlation lengths ξ_1 and ξ_2 are unequal and in general $\xi_2>\xi_1$. ξ_1 remains finite reaching maximum values which range from 10 to 20 Å depending on the compound, while ξ_2 shows a very strong temperature dependence and reaches large values of >500 Å for Y and Ho and appears to saturate near 400 Å for Yb. The temperature dependence of the product $B\xi_2$ is order parameter like. The above behavior is compared to that of reentrant spin glasses but with ferromagnetic and spin glass temperatures nearly coincident. [S0163-1829(96)07034-8]

I. INTRODUCTION

Magnetically frustrated materials have attracted considerable attention recently, particularly those in which the frustration appears to be primarily geometrical or topological in origin rather than induced by positional disorder.[1,2] Such materials often order in unusual, noncollinear magnetic structures, such as the 120° structure found in triangular lattices and exhibit critical exponents which are different from those predicted by universality.[1] In some cases the level of frustration is so extreme that true long range order is never achieved but instead there exists evidence for a transition to a spin-glass-like state. Among the best studied examples of this latter category of compounds are the magnetoplumbite structure oxide, $SrCr_xGa_{12-x}O_{19}$, the garnet $Gd_3Ga_5O_{12}$, and the pyrochlore structure oxide families $R_2Mo_2O_7$ and $R_2Mn_2O_7$, where R is a rare earth.[3–9] In the case of $SrCr_xGa_{12-x}O_{19}$ the geometric frustration arises due to the location of magnetic Cr^{3+} ions on layers with a *kagomé* topology, i.e., corner shared equilateral triangles.[3] Current thinking suggests that the magnetically frustrated unit comprises two *kagomé* layers sandwiching a triangular layer which is equivalent to a bilayer of distorted corner sharing tetrahedra. There exists a detectable level of disorder in this material as Cr^{3+} and Ga^{3+} compete for occupation of the *kagomé* and triangular sites.[3] In $Gd_3Ga_5O_{12}$ the Gd^{3+} sublattice forms two sublattices of three-dimensional corner sharing triangles.[4] As superexchange is very weak between rare

earth ions, long range dipolar coupling is competitive.

The pyrochlore oxides represent a somewhat different situation than the aforementioned materials in that site disorder is generally minimal and that superexchange clearly dominates the magnetic interactions.[5] This report concerns results for three pyrochlore structure oxides, $Ho_2Mn_2O_7$, $Yb_2Mn_2O_7$, and $Y_2Mn_2O_7$. For the latter material a reasonably detailed study already exists.[6,10] Pyrochlore oxides of the composition in question are described in space group $Fd3m$ with R in 16d, Mn in 16c, O1 in 48f, and O2 in 8b.[11] There is generally little evidence for site mixing among the cations or for significant vacancy concentrations on the oxygen sites. This issue will be addressed in more detail for the Ho and Yb materials. Both the 16d and 16c sites independently form three-dimensional arrays of perfect corner sharing tetrahedra and thus there exists the potential for geometric frustration if the nearest neighbor exchange is antiferromagnetic. $Y_2Mn_2O_7$ is the simplest of the three materials as only the 16c site is occupied by magnetic ions. This compound seems to be an unlikely candidate for magnetic frustration as the Weiss constant, $\theta_p = +41$ K, indicating the predominance of ferromagnetic exchange coupling.[12] Nonetheless, dc and ac susceptibility, specific heat, and neutron diffraction studies show no evidence for long range magnetic order of any type and instead a spin-glass-like behavior is seen below 7 K preceded by an apparent ferromagnetic transition at 17 K.[6] Analysis of the diffuse magnetic scattering is consistent with a nearest neighbor antiferromagnetic exchange and ferromagnetic interactions for more distant neighbors. Small angle neutron scattering (SANS) data over a limited Q range indicate that the 17 K ferromagnetic anomaly is due to the formation of finite-size ferromagnetic clusters.[10]

$Ho_2Mn_2O_7$ and $Yb_2Mn_2O_7$ represent more complex cases as there are magnetic ions on the 16d sites as well. Much less is known about these materials except that the Curie-Weiss θ_p values are also positive.[12] In this work the results of a reasonably comprehensive study of $Ho_2Mn_2O_7$ and $Yb_2Mn_2O_7$ including dc and ac susceptibilities, specific heat, and neutron diffraction data are reported. In addition, the magnetic microstructure of these compounds and $Y_2Mn_2O_7$ were examined by SANS over wide ranges of temperature and Q.

II. EXPERIMENT

A. Sample preparation

The sample preparation has been described previously and requires the firing of MnO_2 and R_2O_3 under hydrothermal conditions in a sealed gold tube at 500 °C and 3 kbar pressure.[12] The high pressure is necessary to stabilize the Mn^{4+} oxidation state.

B. Neutron powder diffraction

Neutron powder diffraction data used for the refinement of the crystal structures and for magnetic scattering studies on $Ho_2Mn_2O_7$ and $Yb_2Mn_2O_7$ were obtained at the McMaster Nuclear Reactor using monochromatic neutrons with $\lambda = 1.392$ Å. The position sensitive detector and other experimental details have been described previously.[5]

C. dc susceptibility

dc susceptibility data were obtained using a SQUID magnetometer (Quantum Design, San Diego). Zero-field-cooled (ZFC) susceptibility data were obtained by cooling the sample down to 5 K in a field of less than 0.5 G and measuring at an applied field of 100 G. Field-cooled (FC) data were measured after cooling the sample from room temperature down to 5 K in a field of 100 G.

D. ac susceptibility

Real and imaginary parts, χ' and χ'', of the susceptibility were determined with an ac Lake Shore 7000 susceptometer. The samples were first cooled in the earth's magnetic field and then an ac field was applied ranging from 0.5 to 10 G. For each temperature frequencies ranging from 8 to 222 Hz were used. In order to correct the dephasing angle indicated by Lake Shore, the curves χ''/χ' were plotted with $\theta = 90°$. For the highest temperatures this ratio is approximately constant and equal to $\tan(\theta)$. The angles extracted from these values allow replotting of the susceptibilities with appropriate angle corrections.

E. Specific heat

The specific heat of the samples in the form of powders was measured in the temperature range 2–90 K using a fully automated quasiadiabatic calorimeter equipped with a calibrated Ge thermometer. The apparatus has been described elsewhere.[13] To ensure good thermal conductivity of the powder samples, the powders were placed in a duran glass ampoule and sealed under a helium atmosphere.

F. Small angle neutron scattering (SANS)

The small angle neutron scattering (SANS) experiments were performed at the instrument at the DR3 reactor at Risø National Laboratory.[14] This instrument uses a cold neutron source and it is situated after a 20 m long curved neutron guide in a low background environment. The neutrons are monochromatized by a mechanical velocity selector which in the present experiments was set at a wavelength resolution of 18% (full width at half maximum value). The neutrons are collimated by two circular apertures with diameters of 18 and 8 mm, respectively, for the source and sample apertures. The distance L between the apertures can be varied in steps of 1 m (from 1 to 6 m) and the sample-detector distance can be varied continuously from 1 to 6 m. In the present experiments two settings were used: (i) $\lambda = 6.5$ Å, $L = 1$ m and (ii) $\lambda = 6.5$ Å, $L = 3$ m, where λ is the neutron wavelength. These settings cover the range of scattering vectors Q, from 0.01 to 0.2 Å^{-1}. The samples were held in a He flow cryostat affording temperature control of ± 0.02 K. The magnetic contribution to the total SANS intensity at low temperatures was obtained by point-by-point subtraction of a data set obtained in the paramagnetic state, 50 K for R=Y and 80 K for R=Ho and Yb, where the SANS intensity is due to nuclear scattering and a small background from paramagnetic scattering. For the samples studied here the magnetic contribution at low temperature is quite large relative to the nuclear scattering which arises, presumably, from the grain boundaries and voids in the powders. In the range 0.01–0.2 Å^{-1}

the Q-integrated intensities are 40–50 % greater at 6 K than at 50 K for R=Y and 400% greater at 6 K than at 80 K for R=Ho with intermediate enhancements for R=Yb. The measured intensities were corrected for variations in the efficiency of the two-dimensional position-sensitive detector by dividing the spectrum recorded for water, which is Q independent as it is mainly due to incoherent scattering from hydrogen. Transmission coefficients were in excess of 85% for experimental settings (i) and (ii) indicating the absence of multiple scattering.

III. RESULTS AND DISCUSSION

A. Crystal structure and disorder levels in $Ho_2Mn_2O_7$ and $Yb_2Mn_2O_7$

As mentioned in the Introduction the structure of pyrochlore materials with composition $A_2B_2O_7$ is described in space group $Fd3m$ with A(III) in 16d B(IV) in 16c, O1 in 48f, and O2 in 8b, where the numbers in parentheses represent the formal oxidation states of the cations. As the question of disorder in these materials is of importance it is useful to recall that the pyrochlore structure can be described as an ordered superstructure of the CaF_2 structure. This structure is described in $Fm3m$ and an oxide of composition AO_2 has A(IV) in 4a and O in 8c. To form the ordered pyrochlore supercell the cubic CaF_2 structure is doubled along all three axes and the A sublattice is divided into two equal parts, A and B, which are each distributed over exactly half of the original fcc positions which are the 16c and 16d sites in $Fd3m$. The A and B ions order only when they differ significantly in ionic radius. Empirically, the pyrochlore superstructure is found for a radius ratio A(III)/B(IV)>1.46 in oxide systems and a disordered CaF_2 structure obtains for smaller ratios. In addition the oxygen atoms order as well, driven by the different coordination requirements of A(III) and B(IV). The larger A(III) ion retains eight fold coordination but is highly distorted from the ideal cubic environment of CaF_2 while the B(IV) ion obtains six fold octahedral coordination. The potential 64 oxygen sites of the doubled CaF_2 cell are reduced to 56 since half of the cations are formally in oxidation state (III) and these sites are divided into two sets, 48f, which coordinate both A(III) and B(IV) and 8b which coordinate only A(III). Thus the full composition of the pyrochlore unit cell is $A(III)_{16}B(IV)_{16}O1_{48}O2_8\square_8$, where $\square$ represents vacancies in the oxide sublattice.

In a diffraction experiment this high degree of ordering is manifested in the appearance of reflections (hkl), h, k, and l all odd, and information regarding the extent of order/disorder is contained in these reflections. The neutron powder method is ideally suited to probe these materials as Mn has a negative scattering length, $b=-3.37$ fm, and O, $b=5.80$ fm, has a scattering length comparable to that of the remaining cations, Ho, $b=8.08$ fm, and Yb, $b=12.4$ fm. There is thus a high level of contrast for both cation and oxygen ordering.

In Fig. 1 is shown the neutron powder diffraction pattern for $Yb_2Mn_2O_7$. The reflections marked with an (*) are the h,k,l-odd supercell reflections which are seen to represent the strongest set of reflections in the pattern. The figure also shows the results of a Rietveld fitting of the pattern to the fully ordered model. The appearance of Fig. 1 and the results listed in Table I indicate that the fully ordered model provides an excellent fit to the data. Refinement of a cation disorder parameter indicates a maximum mixing level of 1.2(4)%. A similar analysis of the possibility of oxygen vacancies on either the 48f or 8b sites yields a maximum vacancy concentration of 0.4(2)%. Results for $Ho_2Mn_2O_7$ are similar with a 1.3(7)% limit for cation mixing and 0.6(4)% of oxygen vacancies. According to the above analyses, these are crystallographically well-ordered materials. From analysis of diffraction data it is possible only to set rough upper limits to various defect levels. In any real solid defects will exist at concentrations undetectable by diffraction methods and thus no materials, including these, can be considered to

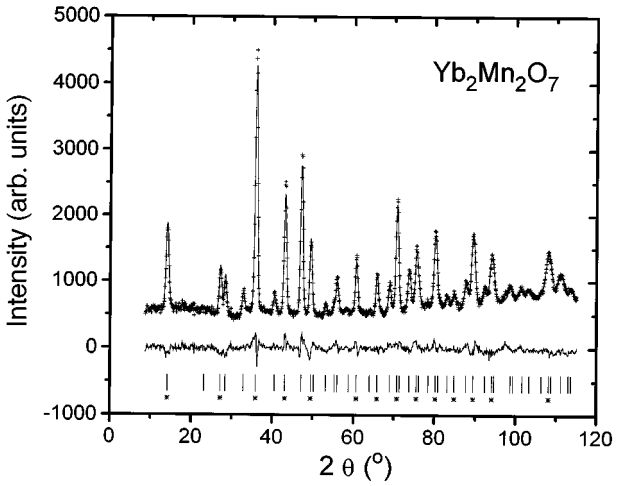

FIG. 1. Powder neutron diffraction data for $Yb_2Mn_2O_7$ at room temperature. Solid line through the data points shows the profile obtained by Rietveld analysis. Lower solid line corresponds to the difference between the fit and the data. Vertical bars indicate the 2θ angles for possible reflections. Marked with an asterisk are the h,k,l- odd supercell reflections.

TABLE I. Results of crystal structure refinements for $R_2Mn_2O_7$ (R=Ho, or Yb) at room temperature.

	Ho	Yb
R (1/2 1/2 1/2)		
B_{iso} (Å^2)	0.44(6)	0.90(5)
Mn (0 0 0)		
B_{iso} (Å^2)	0.2(1)	0.2(1)
O1 (3/8 3/8 3/8)		
B_{iso} (Å^2)	0.3(1)	0.5(1)
O2 (x 1/8 1/8)		
x	0.3277(2)	0.3285(3)
B_{iso} (Å^2)	0.44(4)	0.80(5)
a (Å)	9.907(1)	9.838(1)
Volume (Å^3)	972.470	952.180
R_{wp}	5.49	5.91
R_{exp}	3.37	3.47
χ^2	2.65	2.91
Bragg R factor	8.37	10.2
R-F factor	6.92	6.80

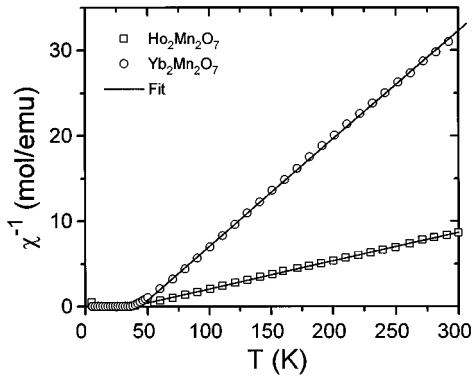

FIG. 2. Inverse molar susceptibilities against temperature for $Yb_2Mn_2O_7$ and $Ho_2Mn_2O_7$. Solid lines represent Curie-Weiss behavior.

be perfectly ordered at the microscopic level. The role of defects at such low levels in the determination of magnetic properties is unclear. In conventional spin glasses defects are the source of the frustration but in the pyrochlore oxides, frustration is geometric in origin and the role of defects may be more subtle. We are not aware of any detailed study of this problem in geometrically frustrated systems and any discussion would be highly speculative at this time.

Indirect evidence for defect levels can be obtained from other sources such as electrical transport. In the original report on these materials all were characterized as insulators with room temperature resistivities in the 10^6–10^8 Ω cm range.[12] The samples used in the present studies are from the same source and have unit cell constants indentical to those in Ref. 12. When carrier levels reach even the level of 10^{-3} per formula unit, as reported for the isostructural $Tl_2Mn_2O_7$, room temperature resistivities drop to the range of 1–10^2 Ω cm.[15] Thus the carrier concentrations in our samples are likely to be considerably below the level of 10^{-3} per formula unit but are not presently known.

B. dc susceptibilities

dc susceptibility data for $Ho_2Mn_2O_7$ and $Yb_2Mn_2O_7$ are similar in appearance; see Fig. 2. Both obey a Curie-Weiss law in the range 60 K$<T<$300 K with positive θ_p intercepts of 37.2(9) and 43.9(8) K for R=Ho and Yb, respectively, in excellent agreement with previous work.[12] Also, the Curie constant values of 30.2(1) and 7.9(2) emu K mol^{-1} for R=Ho and Yb, respectively, are in very good agreement. At low temperatures, Figs. 3(a) and 3(b), both compounds show two features in common, a sharp susceptibility increase just below 40 K accompanied by the appearance of FC-ZFC irreversibilities and broad maxima in the ZFC data at lower temperatures, about 33 K for R=Ho and 23 K for R=Yb. Such results are very similar to those already reported for $Y_2Mn_2O_7$ for which the sharp rise and divergence is at 16 K and the broad maximum is at 7 K.[6] That these features occur in a higher temperature range for R=Ho and Yb is attributable to the additional R-Mn interaction in these materials which is lacking when R=Y.

Magnetic moment as a function of applied field is plotted in Fig. 4 for R=Ho and Yb. Saturation magnetization behaviors are observed with 12.4 μ_B for $Ho_2Mn_2O_7$ and 9.2 μ_B for

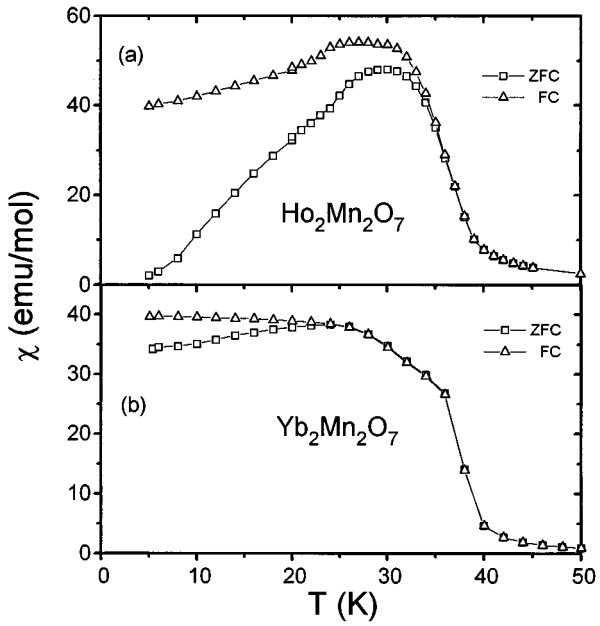

FIG. 3. Zero-field-cooled (ZFC) and field-cooled (FC) susceptibilities for (a) $Ho_2Mn_2O_7$ and (b) $Yb_2Mn_2O_7$ at low temperatures.

$Yb_2Mn_2O_7$ at 5 K for applied fields higher than 1.0 and 0.5 T, respectively. For $Y_2Mn_2O_7$, complete saturation behavior was not observed at similar fields and temperatures.[6] The expected magnetic moments, gJ, for free Ho^{3+} and Yb^{3+} ions are 10.0 μ_B and 4.0 μ_B, respectively. Assuming that the Mn^{4+} sublattice saturates near the theoretical limit of 3.0 μ_B/Mn^{4+} in these materials (S=3/2, $g\approx$2.0) the observed rare earth moments, per atom, are 3.2 μ_B for Ho and 1.6 μ_B for Yb. The smaller observed values in comparison with the expected ones indicate a strong crystal field splitting of the respective ground states, which will be substantiated by the heat capacity results in Sec. III D. In a previous report on isostructural $Yb_2V_2O_7$, the ground state doublet of Yb^{3+} gave rise to a moment of 1.7 μ_B/Yb^{3+} from neutron diffraction and magnetization studies.[16] As the crystal fields at the Yb site in these materials are likely to be very similar, the Yb moments should also be very similar and the agreement is gratifying. This observation supports the assumption that the Mn^{4+} sublattice does saturate with its full value of 3.0 μ_B/Mn^{4+} at high fields and low temperatures. There are no comparable data for any Ho pyrochlore oxide. In summary, the magnetization data for both $Ho_2Mn_2O_7$ and $Yb_2Mn_2O_7$ show saturation behavior at low temperatures and high fields

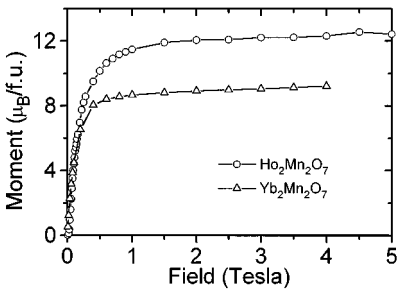

FIG. 4. Magnetization as a function of applied field for $Ho_2Mn_2O_7$ and $Yb_2Mn_2O_7$ at 5.0 K.

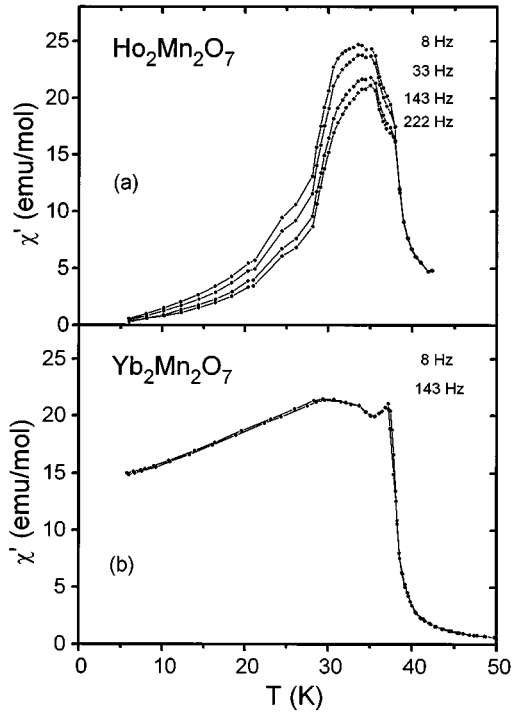

FIG. 5. The real parts of the ac susceptibility measured at different frequencies (increasing from top to bottom) for (a) $Ho_2Mn_2O_7$ and (b) $Yb_2Mn_2O_7$.

with saturation moments which can be understood in terms of a collinear ferromagnetic coupling between the Mn^{4+} and R^{3+} sublattices with a full spin only value for the former and crystal field reduced values for latter.

C. ac susceptibilities

1. $Ho_2Mn_2O_7$

The results are shown in Fig. 5(a) and it is clear that the χ' behavior of this material is quite complex. First, there is a sharp increase in the χ' below 40 K, also seen in the dc data, and a strong frequency dependence which sets in at 38 K, matching the onset of the FC-ZFC divergence in the dc results. A fairly sharp, frequency independent maximum at 35 K is followed by a broader, frequency dependent maximum at about 33 K and then χ' drops rapidly. The presence of a frequency dependent maximum is often taken as a sign of either spin glass or superparamagnetic behavior. To distinguish between these possibilities it is common to compute the quantity

$$K=\frac{\Delta T_g}{T_g \Delta \ln(f)}, \tag{1}$$

where T_g is the maximum in χ', f is the frequency, and Δ refers to differences between measurements at different frequencies.[17] For spin glasses K is found to be of the order of 0.01 while for superparamagnets $K>0.1$.

For $Ho_2Mn_2O_7$, $K=0.015(10)$ which is consistent with the spin glass category. Another property of spin glasses is the dynamical slowing down of the spin fluctuations near the glass transition temperature which has the well-known power law dependence

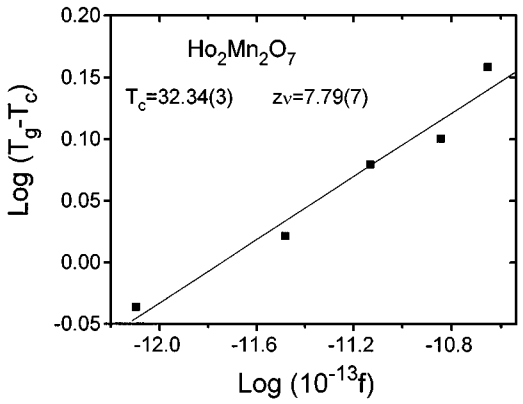

FIG. 6. Log-log plot of the frequency dependence of (T_g-T_c) for $Ho_2Mn_2O_7$.

$$\tau=\tau_0\left(\frac{T}{T_c}-1\right)^{-z\nu}, \tag{2}$$

where τ is the measured relaxation time, z and ν are critical exponents, and τ_0 is usually taken as 10^{-13} sec.[17] A more convenient form for comparison with experiment is

$$T_g=T_c[1+(\tau_0 f)^{1/z\nu}]. \tag{3}$$

Analysis of the data of $Ho_2Mn_2O_7$ according to (3), shown in Fig. 6, yields $T_c=32.34(3)$ and $z\nu=7.79(7)$. These critical exponents are typical for spin glasses.

2. $Yb_2Mn_2O_7$

Corresponding data for this material, Fig. 5(b), show much less dramatic frequency dependence, but similar features. There is a sharp rise in χ' and the onset of frequency dependence at 38 K with a sharp cusp which is followed by a very broad maximum near 30 K. As the frequency dependence of this sample was much weaker, no attempt was made to carry out a quantitative analysis.

3. $Y_2Mn_2O_7$

The frequency dependence of χ' for this material has already been noted in Ref. 6. Interestingly, while a monotonic increase in $\chi'_{\max}$ occurs with increasing frequency, there exists an apparent saturation above about 200 Hz. Analysis of the data of Ref. 6 in the frequency range 10–200 Hz in terms of (1) gives $K=0.0365(5)$ which is clearly in the spin glass regime. An attempt to extract critical exponents by fitting to (2) was unsuccessful with any physically reasonable value for τ_0. A more detailed experimental study and analysis, including both χ' and χ'', is currently underway.

In summary of this section there is good evidence for both $Ho_2Mn_2O_7$ and $Y_2Mn_2O_7$ for spin glass rather than superparamagnetic behavior. The situation is less clear for $Yb_2Mn_2O_7$.

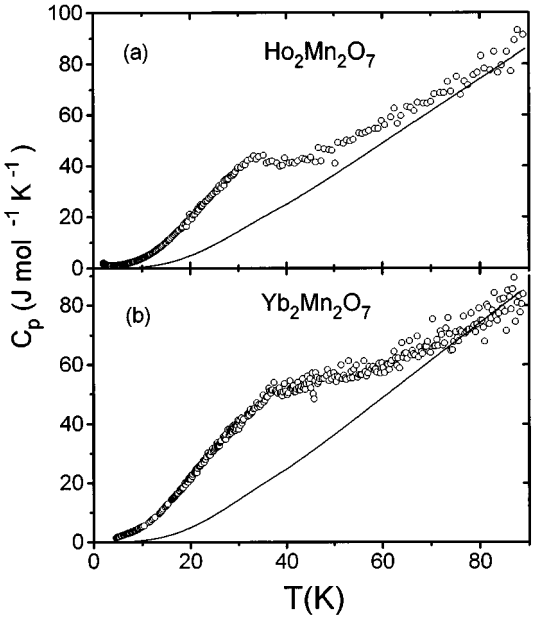

FIG. 7. Measured specific specific heat, C_p, of (a) $Ho_2Mn_2O_7$ and (b) $Yb_2Mn_2O_7$. Solid lines represent the corresponding lattice specific heats.

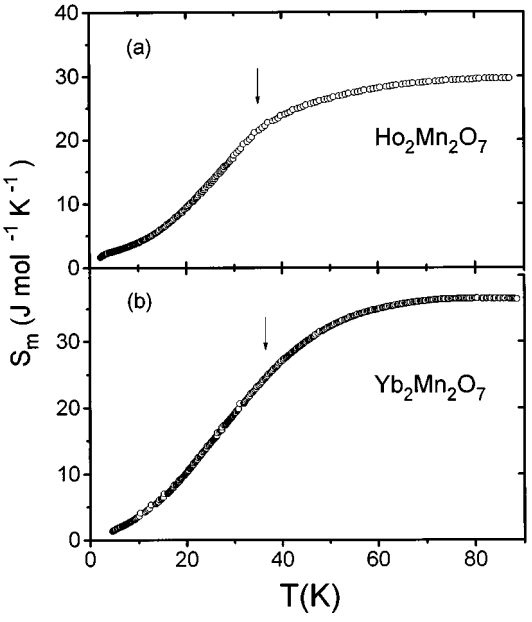

FIG. 9. Development of magnetic entropy with temperature for (a) $Ho_2Mn_2O_7$ and (b) $Yb_2Mn_2O_7$. Arrows mark the transition temperatures.

D. Heat capacity

Results for both $Ho_2Mn_2O_7$ and $Yb_2Mn_2O_7$ are shown in Figs. 7(a) and 7(b) for a reasonably wide temperature range. In both cases the magnetic contributions, Figs. 8(a) and 8(b), are dominated by a very broad feature, peaked near 35 K for R=Ho and slightly higher at 38 K for R=Yb, but extending over the entire temperature range investigated. There is, thus, no evidence for a λ-type anomaly which would be indicative of true long range magnetic order in these materials. This is in contrast to the situation for the related vanadium pyrochlores, $Lu_2V_2O_7$ and $Yb_2V_2O_7$, where a sharp, λ-type feature is seen.[18] The magnetic heat capacity for both $Ho_2Mn_2O_7$ and $Yb_2Mn_2O_7$ is however, more sharply peaked than that of $Y_2Mn_2O_7$ (Ref. 6) indicating, perhaps, a longer correlation length in the former materials but still no true long range magnetic order.

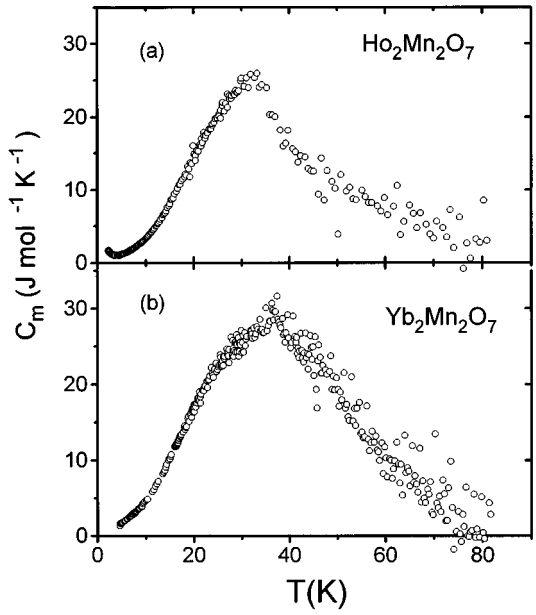

FIG. 8. Magnetic specific heat, C_m, of (a) $Ho_2Mn_2O_7$ and (b) $Yb_2Mn_2O_7$.

Figures 9(a) and 9(b) show the temperature dependence of the magnetic entropy for both materials. At 90 K the entropy gains are 30 and 37 J mol^{-1} K^{-1} for R=Ho and Yb, respectively. These can be compared with values calculated assuming free ion behavior for the rare earths, Ho^{3+}, $^5I_8$, Yb^{3+}, $^2F_{7/2}$ and spin only behavior for Mn^{4+}, S=3/2 using the standard expression

$$S = 2R[\ln(2J+1) + \ln(2S+1)]. \quad (4)$$

The calculated values are 70.2 and 57.6 J mol^{-1} K^{-1} for $Ho_2Mn_2O_7$ and $Yb_2Mn_2O_7$, respectively. Clearly, the entropy gains are very much smaller than expected on the basis of Eq. (4). The magnetic entropy of $Y_2Mn_2O_7$, where only Mn^{4+} is magnetic, reaches 45% of its expected value (R ln 4 =11.5 J mol^{-1} K^{-1}) at T_c, where magnetic data shows spontaneous magnetization, and close to its full value around 90 K, well above the T_c.[6] The magnetic entropy values of spin-glass-like pyrochlores $Sm_2Mo_2O_7$ and $Gd_2Mo_2O_7$ corresponds to a two-level and an eight-level ground state for Sm^{3+} and Gd^{3+} ions, respectively.[7] Sm^{3+} develops a Kramer's doublet magnetic ground state as the crystal field removes the degeneracy of $^6H_{5/2}$ ground state. However, Gd^{3+} ion with an isotropic ground state $^8S_{7/2}$ is not much affected by the crystal fields. Also, in yet another pyrochlore $Yb_2V_2O_7$, where a long-range magnetic ordering occurs below 70 K, Yb^{3+} has a doublet magnetic ground state.[16]

From these evidences, it may be assumed that Ho^{3+} and Yb^{3+} ions in $Ho_2Mn_2O_7$ and $Yb_2Mn_2O_7$, respectively, have doublet ground states and Mn^{4+} has a quartet. The total expected magnetic entropy for $R_2Mn_2O_7$ (R=Ho, Yb) with

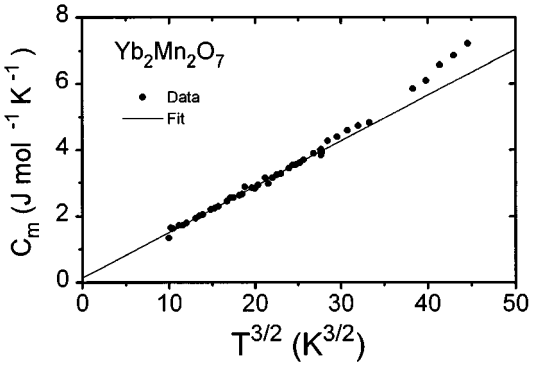

FIG. 10. Magnetic specific heat, C_m, versus $T^{3/2}$ for $Yb_2Mn_2O_7$ at low temperatures.

such a scheme of ground states is 35 J mol^{-1} K^{-1}. The magnetic entropy of $Ho_2Mn_2O_7$ reaches 64% of this expected value at T_c and 86% at 90 K indicating the presence of short range interactions well above the T_c. On the other hand, the magnetic entropy of $Yb_2Mn_2O_7$ reaches 69% of the expected value at T_c and 36.4 J mol^{-1} K^{-1} at 90 K, slightly higher than the expected value. This small discrepancy could either be due to the errors involved in estimating the lattice part of the heat capacity or the weak contributions from the levels above the doublet. In summary, the heat capacity studies of $R_2Mn_2O_7$ (R=Ho, Yb) indicate (i) the absence of true long range magnetic order, (ii) the presence of short range interactions well above the T_c, and (iii) doublet ground states for Ho^{3+} and Yb^{3+} ions as for the other rare earths in related pyrochlores.

It is important to determine the temperature dependence of the heat capacity. In the low temperature regime for $Y_2Mn_2O_7$ a linear dependence of C_m on T was observed below about 7 K which is often regarded as the definitive result for spin glass materials. On the other hand, a $T^{3/2}$ dependence has also been observed in systems usually regarded as canonical spin glasses.[19] Figure 10 shows the magnetic heat capacity of $Yb_2Mn_2O_7$ as a function of $T^{3/2}$ in the temperature range 15–4 K. It is evident that a $T^{3/2}$ behavior holds from 11 to 4 K. It is noted that the onset temperature for this power law behavior corresponds to roughly 0.3 T_g, which is consistent with reports for other spin glass systems.[19] Our results also show a T=0 K intercept of about 0.14(4) J mol^{-1} K^{-1}, a feature also seen in the canonical systems.[19] It has been speculated that this excess heat capacity is associated with the unblocking of the remnant magnetization. Unfortunately, the appearance of a $T^{3/2}$ dependence is not subject to unambiguous interpretation, as this is also the result expected for a material in which spin wave type excitations exist. Evidence from neutron scattering in the next two sections suggests such a possibility for $Yb_2Mn_2O_7$.

A similar analysis cannot be carried out for $Ho_2Mn_2O_7$ due to the increase in heat capacity evident at low temperatures; see Fig. 8(a). This increase may be the source of some of the missing entropy in this material and measurements to lower temperatures are planned.

E. Low temperature neutron diffraction

1. $Ho_2Mn_2O_7$

Figure 11 shows the temperature dependence of the low angle part of the neutron powder diffraction pattern for

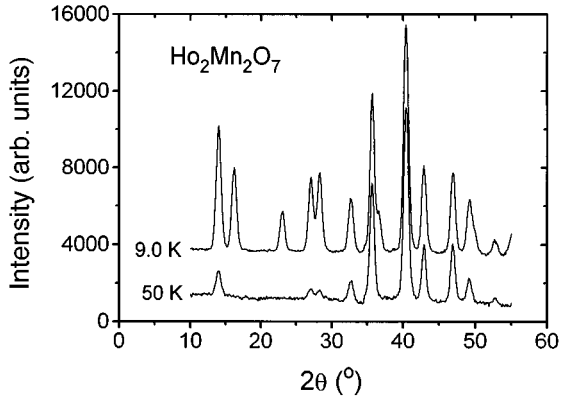

FIG. 11. Low angle powder neutron diffraction profiles for $Ho_2Mn_2O_7$ at 9 and 50 K.

$Ho_2Mn_2O_7$ and Fig. 12 the difference plot for the 9 and 50 K data. Two features are immediately apparent. First, the temperature dependent reflections are coincident with those of the chemical unit cell although two reflections, (200) and (420), violate the d-glide symmetry. Second, and remarkably, all of the reflections are enhanced, there are apparently no systematics and indeed from Fig. 12 the intensities fall roughly as expected from the magnetic form factor behavior. In addition a detailed examination of the reflection widths shows no change within the temperature range investigated, i.e., the reflections are resolution limited at all temperatures. From the resolution of the data a minimum correlation length of about 100 Å can be estimated. The second observation, the nearly uniform distribution of magnetic scattering among the various Bragg peaks, is unprecedented for pyrochlore materials and is not consistent with any simple collinear or approximately collinear magnetic structure involving ferro or ferrimagnetic coupling between the Ho and Mn sublattices nor the so-called 109° structure where moments are directed toward the corners of the tetrahedra comprising both magnetic sublattices wherein the (hhh) reflections are systematically absent.[8,20]

An attempt was made to determine the magnetic structure at 9 K by Rietveld analysis. Although a satisfactory solution for the magnetic structure could not be found, it was ob-

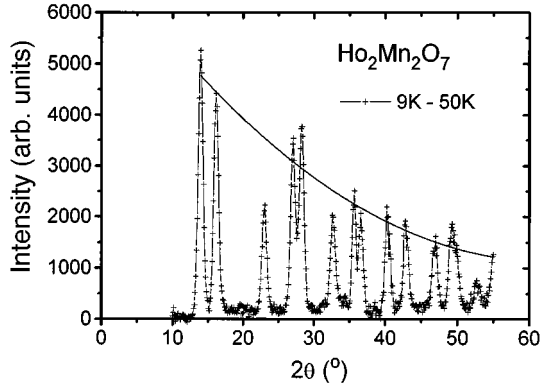

FIG. 12. Differences in the intensities of powder neutron diffraction data between 9 and 50 K for $Ho_2Mn_2O_7$. Solid line is to signify that the fall of intensities against 2θ is similar to that of the magnetic form factor.

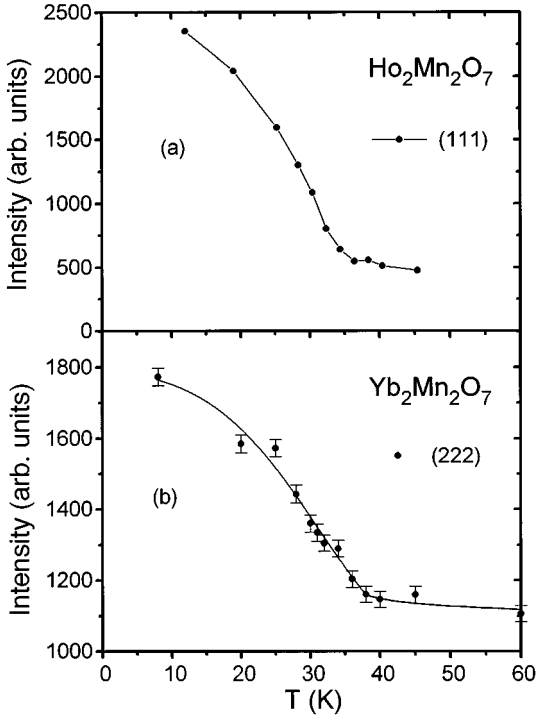

FIG. 13. (a) The temperature dependence of the intensity of the reflection (111) for $Ho_2Mn_2O_7$. (b) The temperature dependence of the intensity of the reflection (222) for $Yb_2Mn_2O_7$.

served that a configuration of nearest neighbor Ho spins with a canting angle of ~110° and *nn* Mn spins with a canting angle of ~75° lying in the *a*-*b* plane generate magnetic intensity in the (200) and (420) reflections which are forbidden for collinear magnetic structures. However, these canting angles are not necessarily unique but do indicate the canted nature of magnetic order in $Ho_2Mn_2O_7$.

The temperature evolution of the intensity of the (111) reflection is shown in Fig. 13(a). This has the appearance of an order parameter and is consistent with a critical temperature near 35 K. Heat capacity data indicate that the ordering involved cannot be of long range and indeed there is a correlation with the spin glass temperature determined earlier. Such behavior has been seen in other spin glass systems as will be discussed later, and is attributed to the formation of spin-canted domains.

2. $Yb_2Mn_2O_7$

Neutron diffraction data at 8 and 60 K are shown in Fig. 14. In sharp contrast to $Ho_2Mn_2O_7$, only two Bragg reflections, (222) and (004), indicated by arrows in the figure, are enhanced due to magnetic ordering. The temperature variation of the intensity of the magnetic reflection (222), as shown in Fig. 13(b), also appears to be order parameter like with an onset temperature of ~37 K. Magnetic structure analysis of the data at 8 K indicates a collinear FM coupling of the two sublattices with 0.6(1) μ_B/Yb^{3+} and 1.7(2) μ_B/Mn^{4+}. The structure refinement results are found to be independent of the spin orientation with respect to the crystal lattice demonstrating the isotropic nature of the exchange coupling. The refined magnetic moment values at zero applied field are only ~40% and ~60% of the ones deduced

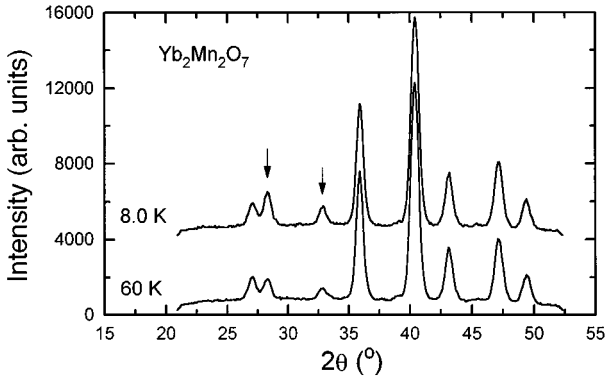

FIG. 14. Powder neutron diffraction profiles for $Yb_2Mn_2O_7$ at 8 and 60 K.

from the saturation magnetization data at modest fields for Yb^{3+} and Mn^{4+}, respectively. This suggests a more complex situation than a collinear structure which may take the form of sublattice canting or the coexistence of short and long range order although there is no clear evidence for diffuse scattering around any of the Bragg peaks. These results should also be compared with those for the isostructural $Yb_2V_2O_7$ where heat capacity, magnetization and neutron diffraction are consistent with a long range ferromagnetic coupling between Yb^{3+} and V^{4+} with the full moment values for both species in zero field.[16]

In contrast to the above the results for $Y_2Mn_2O_7$ reported previously showed, primarily, diffuse magnetic scattering with an onset near 15 K, the point below which the magnetic susceptibility anomalies set in.[6] The diffuse scattering is centered about the (111) and (113) nuclear reflections. At lower temperatures, near 7 K, weak narrow components appear to be present as well but their significance is ambiguous as the sharp components are superimposed on relatively strong nuclear peaks and the weak resultant feature could be an artifact of the subtraction process. The presence of a predominant diffuse scattering is consistent with the heat capacity data which is not significantly peaked for $Y_2Mn_2O_7$ unlike the situation for $Ho_2Mn_2O_7$, and $Yb_2Mn_2O_7$.

To summarize this section the low temperature neutron diffraction data for R=Ho and Yb phases together with the heat capacity results are consistent with the onset of some as yet unidentified form of intermediate range magnetic order with a strong component of spin canting and a minimum correlation length of about 100 Å. Apparent critical temperatures are ~35 and ~37 K, respectively, for R=Ho and Yb.

F. Small angle neutron scattering (SANS)

Figures 15(a)–15(c) display the temperature variation of the magnetic component of the SANS for each material studied for a range of Q values. In all three cases the trends are similar. For large Q the SANS data mimic the susceptibility results, showing a cusp at 17 K for R=Y and 38 K for R=Yb with a broad maximum for R=Ho. These features disappear gradually with decreasing Q until for the smallest Q all three materials show a steep increase followed by apparent saturation at low temperatures. In all cases the low temperature scattering at small Q exceeds that at large Q,

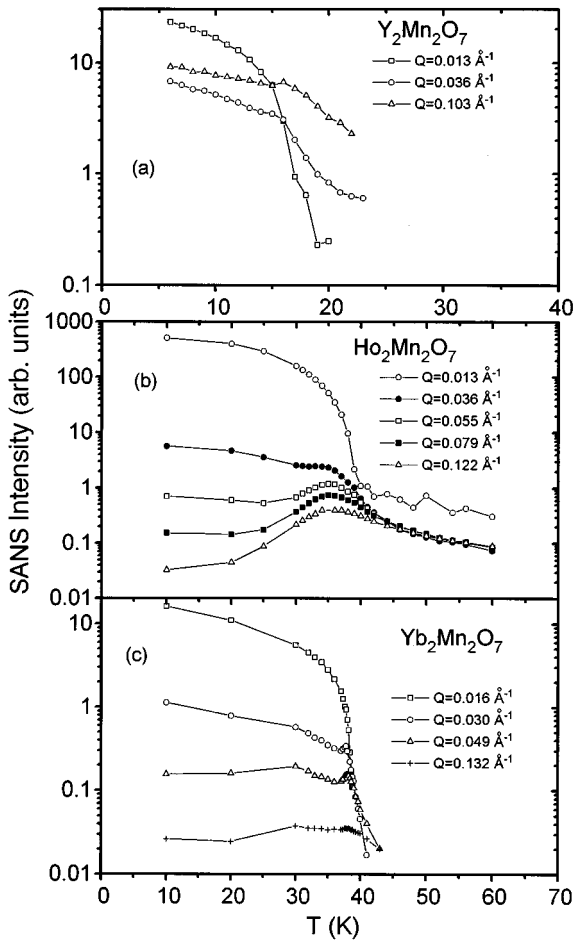

FIG. 15. Magnetic SANS intensities against temperature obtained at different Q values for (a) $Y_2Mn_2O_7$, (b) $Ho_2Mn_2O_7$, and (c) $Yb_2Mn_2O_7$.

often by several orders of magnitude as for R=Ho and Yb. These results contrast sharply with the behavior seen for other pyrochlore oxides such as $Tl_2Mn_2O_{7-x}$ (Ref. 15) and $Nd_2Mo_2O_7$.[8] The former phase is a long range ordered ferromagnet which displays the classic increase in SANS upon approaching T_c from above followed by a decrease to lower temperatures which reflects, first, a build up of subcritical clusters followed by a decrease in their population as the infinite cluster grows below T_c. $Nd_2Mo_2O_7$, a long range ordered ferrimagnet, shows parallel behavior. Clearly, the SANS data for the three $R_2Mn_2O_7$ pyrochlores are not consistent with true long range order and thus are in accord with the susceptibility and specific heat results.

It is possible to obtain a more detailed description of the magnetic microstructure from analysis of the Q dependence of the SANS data. A preliminary report on $Y_2Mn_2O_7$ using relatively high Q data, indicated a reasonable fit to a simple Lorentzian

$$I(Q)=\frac{A}{(Q^2+1/\xi^2)}, \tag{5}$$

where A is a constant and ξ is a correlation length.[10] These observations were interpreted conventionally, i.e., as evidence for the formation of finite ferromagnetic clusters near

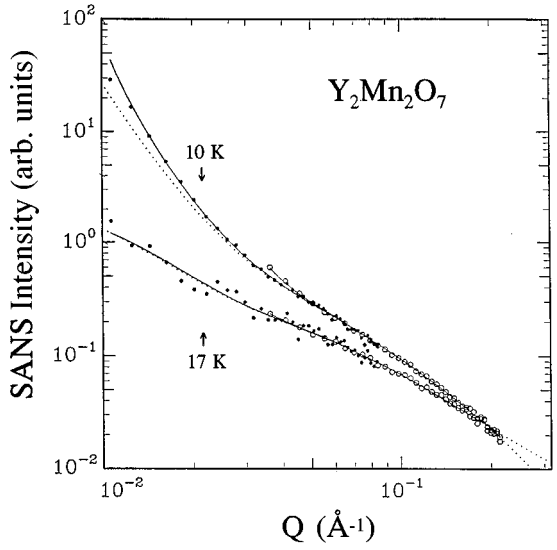

FIG. 16. Q dependence of the magnetic SANS intensities at 10 and 17 K for $Y_2Mn_2O_7$. The open and solid symbols represent the data obtained with the experimental settings (i) and (ii), respectively (for details see Sec. II F in the text). The solid lines and dotted lines are fits to Eq. (6) including the resolution function and without including the resolution function, respectively. For details, see Ref. 22.

the susceptibility anomaly at 17 K. The present data which span a much wider Q and temperature range allow a more thorough analysis for $Y_2Mn_2O_7$ and the other materials as well. The observed scattered intensity for all three materials can be well fitted to the following model which is a sum of a Lorentzian (L) and a Lorentzian-squared (L^2) term:

$$I(Q)=\frac{A}{(Q^2+1/\xi_1^2)}+\frac{B}{(Q^2+1/\xi_2^2)^2}, \tag{6}$$

where B is an additional constant and ξ_1 and ξ_2 are correlation lengths associated with the L and L^2 terms, respectively. The fitting procedures were based on the detailed procedures given in Refs. 21 and 22. Some results for $Y_2Mn_2O_7$ are shown in Fig. 16. Note that for large Q the intensity varies as Q^{-2} while at small Q the dependence approaches Q^{-4} which is consistent with Eq. (6). Such a model cross section is commonly found for spins glass materials including metallic glasses and site-disordered insulators.[23,24]

For the case $\xi_1=\xi_2$ there exists a theoretical justification due to Aharony and Pytte based on a random anisotropy field the influence of which is reflected in the presence of the L^2 term.[25] It has been argued that the same cross section should be expected for the case of random or competing exchange fields. There exists at least one anomalous case where $\xi_1\neq\xi_2$.[26] No detailed theory is available for this situation. In the case cited,[26] in fact ξ_2 was found to be essentially resolution limited over the entire temperature range investigated, i.e., the L^2 term could be replaced with B/Q^4. This is not the case for the materials studied here.

The temperature dependence of the four adjustable parameters in (6) is displayed in Figs. 17(a)–17(c) (the correlation lengths ξ_1 and ξ_2), Fig. 18 (the coefficients A) and Fig. 19 (the coefficients B). Note first that in all three cases, the

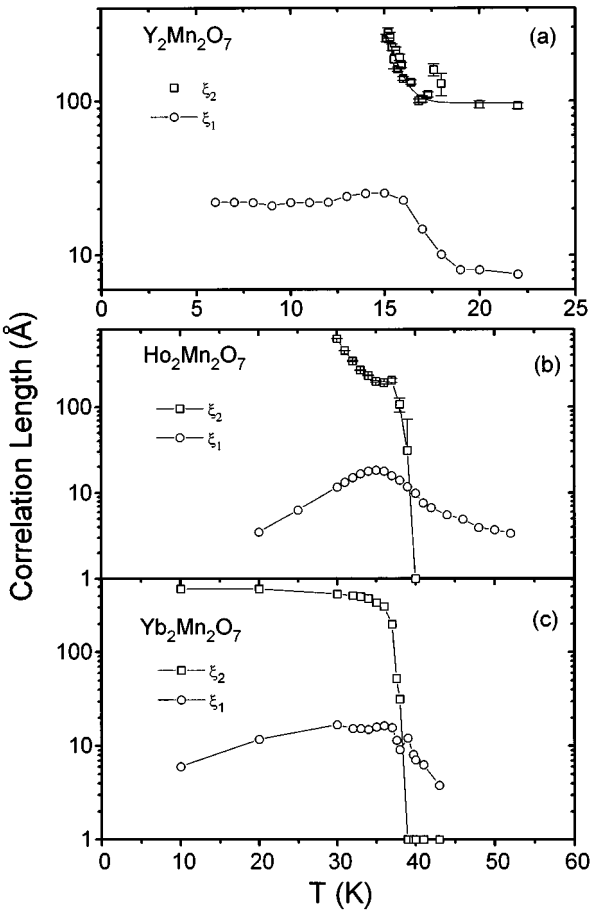

FIG. 17. Correlations lengths, ξ_1 and ξ_2, determined from Eq. (6) for (a) $Y_2Mn_2O_7$, (b) $Ho_2Mn_2O_7$, and (c) $Yb_2Mn_2O_7$.

two correlation lengths are unequal and that $\xi_2 > \xi_1$ in general. It was not possible to fit data over the full Q range available with the constraint $\xi_1 = \xi_2$, the large Q data more or less fix ξ_1 and the small Q data ξ_2. Secondly, the temperature dependencies are strikingly different. In all three cases ξ_1 increases gradually with decreasing temperature from nonzero values well above the apparent spin glass temperatures, then passes through a broad maximum of 25 Å (R=Y) or

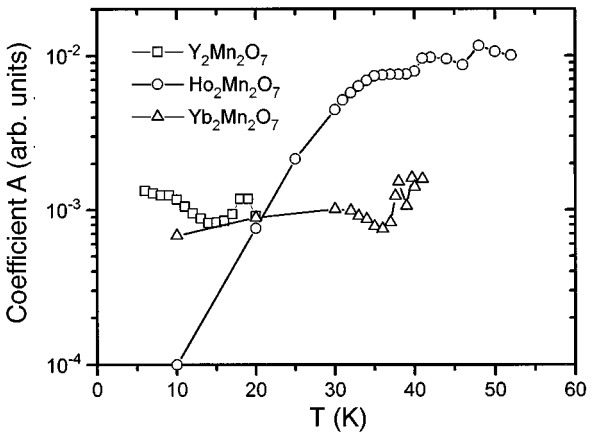

FIG. 18. Coefficients A in Eq. (6) against temperature for $Y_2Mn_2O_7$, $Ho_2Mn_2O_7$, and $Yb_2Mn_2O_7$.

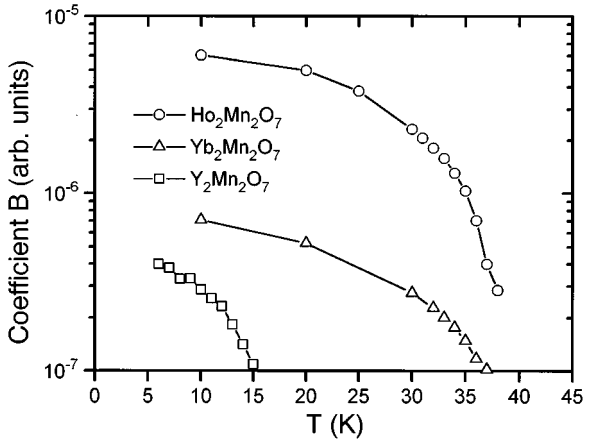

FIG. 19. Coefficients B in Eq. (6) against temperature for $Y_2Mn_2O_7$, $Ho_2Mn_2O_7$, and $Yb_2Mn_2O_7$.

about 10–18 Å (R=Yb and Ho), and finally saturates at lower temperatures (R=Y) or decreases (R=Ho, Yb).

It should be commented here, that for R=Y, the ξ_1 values reported earlier are considerably greater than those found here.[10] This is due, primarily, to the restricted Q range (0.025–0.07 $Å^{-1}$) of the previous study, which, unfortunately, overlaps slightly the regime in which the L^2 term becomes important and to the relatively greater scatter in the data. Both factors contribute to an overestimation of ξ_1 when the data are analyzed with only the L term present.

ξ_2 in contrast shows a very strong temperature dependence with steep increases over very narrow temperature ranges to values exceeding 300–600 Å, depending upon the material. For R=Y and Ho ξ_2 reaches resolution limited values below 15 K (R=Y) and 30 K (R=Ho) and for R=Yb a saturation at about 500 Å.

The temperature dependence of ξ_1 can be compared with similar results for nearly ferromagnetic metallic glasses such as Zr_9Fe_{91}, $NdFe_2$, and Tb_2Fe_{98}, which show a similar broad maximum.[23,27] The most straightforward interpretation is that ξ_1 measures the evolution of ferromagnetic correlations and, clearly, these grow as for a conventional critical phase transition approached from above T_c but an infinite cluster and a true long range order and associated critical temperature are never realized due to the intervention of random fields. The random fields may be of anisotropy or exchange origin or both. It was argued that rounded maxima are characteristic of random exchange fields but anisotropy fields for the R=Ho and Yb materials must play a role as well.

The temperature dependence of the random field component is monitored by the L^2 term and thus ξ_2 and B. In all cases ξ_2 undergoes a steep increase at temperatures just above the maximum in ξ_1, evidence for the competition between the ferromagnetic and random tendencies. It should also be noted that the spin glass signature behaviors in the bulk susceptibilities, such FC-ZFC irreversibilities and frequency dependencies, set in over the temperature interval within which ξ_2 increases dramatically. There is one apparent difference between the behavior of the R=Y phase and the other two materials, in that for the former, ξ_2 attains finite values even above any spin glass transition temperature while for the others the L^2 term and ξ_2 are nearly zero until the spin glass transition.

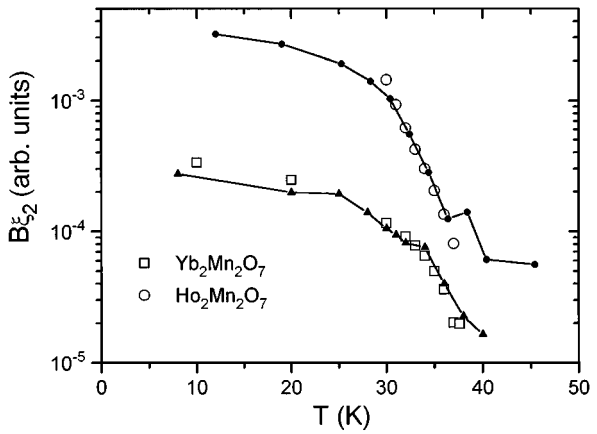

FIG. 20. Product $B\xi_2$ as a function of temperature for $Yb_2Mn_2O_7$ and $Ho_2Mn_2O_7$. Open symbols represent the $B\xi_2$ data. Solid symbols represent the scaled magnetic Bragg peak intensities. Solid lines are guides to the eye.

The coefficients of the L and L^2 terms, A and B, respectively, also present a sharp contrast. The temperature dependence of A is generally rather weak with only small features appearing near the spin glass onset temperatures, although a sharper decrease is evident for R=Ho at lower temperatures. B on the other hand, shows a systematic, order-parameter-like increase below the spin glass onset temperatures for all three materials. In fact it is the quantity $B\xi_2$ which should behave as an order parameter for a spin glass transition.[23,25] This quantity is compared, suitably scaled, to the measured intensity of the magnetic reflections seen for R=Ho and Yb and the agreement is quite good as shown in Fig. 20.

In fact the common behavior of the pyrochlore manganates resembles that seen for reentrant spin glasses with the exception that the ferromagnetic and spin glass transition temperatures are nearly coincident. Among several such systems that of the site disordered crystalline spin glass $(1-x)FeTiO_3(x)Fe_2O_3$ with $x=0.21$ provides particularly strong parallels.[24] Here T_c(ferro) is about 220 K while T_g(spin glass) is about 80 K. SANS and conventional high-Q neutron diffraction have been carried out on this system. The SANS data were analyzed using Eq. (6) with $\xi_1=\xi_2$. It was found that the L term was important only in the range 300–100 K, peaking near the apparent T_c, while the L^2 term dominated below 100 K, rising sharply near T_g. The correlation lengths extracted behave essentially as those for the pyrochlores. (As single crystals were used in that study it was possible to measure parallel and perpendicular components separately while for the pyrochlores only powder averaged values are seen.) ξ measured from the L-dominated high temperature data, which compares to ξ_1 for the pyrochlores, increased to a maximum of about 300 Å near T_c and descended to about 200 Å just above 100 K. Below 100 K the correlation length, which would correspond to ξ_2 for the pyrochlores, increased sharply and reached resolution-limited values of about 1000 Å near T_g. The microstructure in the spin glass state was proposed to consist of large domains which are randomly spin canted with respect to each other. Evidence for spin canting was seen in this system also in the high Q magnetic Bragg scattering involving several reflections which become strongly enhanced below T_g. This is another parallel to the situation reported in the previous section for the R=Ho and Yb pyrochlores in which the magnetic Bragg reflections correlate with the spin glass temperature and for which the magnetic structure must involve spin canting. Spin canting is a common feature of reentrant spin glass transitions and has been seen in many other systems as well.[24]

The picture of the magnetic microstructure which emerges from the neutron scattering data, both SANS and high Q diffraction, must therefore be similar to that seen for more conventional spin glasses, that is, consisting of relatively large randomly spin-canted domains, but more heterogeneous in that smaller ferromagnetic domains apparently coexist within the same temperature range.

IV. SUMMARY

In this work, we have reported a wide variety of studies (i.e., ac and dc susceptibilities, magnetization, heat capacity, neutron diffraction, and small angle neutron scattering) on the frustrated pyrochlores $R_2Mn_2O_7$ (R=Y, Ho, or Yb). These compounds show magnetic transitions with a sharp rise in magnetization below ~20 K (R=Y) and ~40 K (R=Ho, or Yb). Paramagnetic susceptibility data obey Curie-Weiss behavior over a wide temperature range with $+ve\,\theta_p$ values of about 40 K for all three samples indicating ferromagnetic ordering. However, further studies do not substantiate long range order. Qualitative and quantitative dependences of ac susceptibility on frequency for R=Y and Ho are in accord with spin glass behavior. In the case of R=Yb, the frequency dependence is too weak to attempt any analysis.

Previous heat capacity studies of $Y_2Mn_2O_7$ do not show any anomaly at the magnetic transition temperature. A linear behavior of the magnetic specific heat at low temperatures and magnetic entropy considerations clearly suggest spin-glass-like ordering. These were substantiated by the absence of magnetic Bragg peaks below the ordering temperature. On the other hand, conflicting results were obtained for R=Ho and Yb. For instance, the magnetic Bragg peaks, particularly for Ho, are strongly enhanced below T_c suggesting long-range order, but heat capacity fails to show a sharp λ-type anomaly. Rather, the broad magnetic heat capacity anomaly centered around the apparent T_c, and the magnetic entropy development imply short-range ordering. The magnetic Bragg reflection pattern for $Ho_2Mn_2O_7$ is not consistent with any simple collinear or approximately collinear magnetic structure involving ferro or ferrimagnetic coupling between the Ho and Mn sublattice nor the so-called 109° structure. It was observed that a strong canting of the Ho and Mn moments could account for the most unusual feature of the structure, namely the enhancement of all the nuclear Bragg reflections but a unique structure solution was not found. For Yb in contrast only two reflections were magnetically enhanced and a magnetic structure analysis suggests a FM coupling of the two sublattices, namely Yb and Mn. However, the moments obtained at zero field are significantly smaller than those inferred from the saturation magnetization at high fields and it appears that a more complex situation, such as spin canting, is probable. Heat capacity and low temperature neutron diffraction results, together, suggest an intermediate range magnetic order with spin canting and a minimum cor-

relation length of about 100 Å.

SANS data of $Ho_2Mn_2O_7$, $Yb_2Mn_2O_7$, and $Y_2Mn_2O_7$ are also consistent with the lack of true long range order as the intensity at low Q increases with decreasing temperature. A detailed analysis of the Q dependence requires a model cross section containing both a Lorentzian (L) and a Lorentzian squared (L^2) term to fit the data over the full Q range. In all three cases, the correlation lengths ξ_1 (L) and ξ_2 (L^2) differ greatly in magnitude ($\xi_2 > \xi_1$) and in temperature dependence. ξ_1 which is associated with ferromagnetic clusters increases with decreasing temperature from well above the apparent ordering temperatures, and then saturates following a broad maximum at low temperatures for R=Y or decreases for R=Ho and Yb. In all three cases the maximum ξ_1 is between 10–20 Å. In contrast, ξ_2 rises steeply with a decrease in temperature near the apparent T_c's and exceeds values of 300–600 Å. Such behavior is commonly observed in reentrant spin glasses with the exception that in the pyrochlore $R_2Mn_2O_7$ (R=Y, Ho, or Yb) materials both the ferromagnetic and spin-glass orderings are nearly coincident. Strong parallels with the site-disordered spin glass $FeTiO_3$-Fe_2O_3 are identified. Thus the picture of the magnetic microstructure of the site-ordered pyrochlores, deduced from a wide variety of studies, is quite complex consisting of coexisting random spin-canted domains and smaller ferromagnetic domains. Such complex behavior is unprecedented in materials which are crystallographically well ordered. The issue which remains is whether purely geometrical frustration can be solely responsible or whether one must also consider the role of defects at nearly imperceptible concentrations. As mentioned previously, this is a very open question at present and it is hoped that these results will stimulate further work.

ACKNOWLEDGMENTS

J.E.G. acknowledges the support of the Natural Science and Engineering Research Council of Canada, the C.N.R.S. through an appointment as Chercheur Associé and the hospitality of the Laboratoire CRISMAT and the Centre des Matériaux Supraconducteurs. The work at Risø was carried out with the support from the E.E.C. Large Installations Program. We thank C. V. Stager for use of the SQUID magnetometer and McMaster University for direct support of the McMaster Nuclear Reactor.

[1] B. D. Gaulin, in *Magnetic Systems with Competing Interactions (Frustrated Spin Systems)*, edited by H. T. Diep (World Scientific, Singapore, 1994), pp. 286–326; Michel J. P. Gingras, *ibid.*, pp. 238–285.

[2] A. P. Ramirez, Annu. Rev. Mater. Sci. **24**, 453 (1994) and references therein.

[3] X. Obradors, A. Labarta, A. Isalgue, J. Tejada, J. Rodriguez, and M. Pernet, Solid State Commun. **65**, 189 (1988); A. P. Ramirez, G. P. Espinosa, and A. S. Cooper, Phys. Rev. Lett. **64**, 2070 (1990).

[4] P. Schiffer, A. P. Ramirez, D. A. Huse, P. L. Gammel, U. Yaron, D. J. Bishop, and A. J. Valentino, Phys. Rev. Lett. **74**, 2379 (1995).

[5] J. N. Reimers, J. E. Greedan, and M. Sato, J. Solid State Chem. **72**, 390 (1988).

[6] J. N. Reimers, J. E. Greedan, R. K. Kremer, E. Gmelin, and M. A. Subramanian, Phys. Rev. B **43**, 3387 (1991).

[7] N. P. Raju, E. Gmelin, and R. K. Kremer, Phys. Rev. B **46**, 5405 (1992) and references therein.

[8] J. E. Greedan, J. N. Reimers, C. V. Stager, and S. L. Penny, Phys. Rev. B **43**, 5682 (1991) and references therein.

[9] B. D. Gaulin, J. N. Reimers, T. E. Mason, J. E. Greedan, and Z. Tun, Phys. Rev. Lett. **69**, 3244 (1992).

[10] J. E. Greedan, J. Avelar, and M. A. Subramanian, Solid State Commun. **82**, 797 (1992).

[11] M. A. Subramanian, G. Aravamudan, and G. V. Subba Rao, Prog. Solid State Chem. **15**, 55 (1983).

[12] M. A. Subramanian, C. C. Torardi, D. C. Johnson, J. Pannetier, and A. W. Sleight, J. Solid State Chem. **72**, 24 (1988).

[13] E. Gmelin and P. Roedhammer, J. Phys. E **14**, 223 (1981).

[14] J. S. Pedersen, in *Modern Aspects of Small-Angle Scattering*, edited by H. Brumberger (Kluwer Academic, Dordrect, The Netherlands, 1995), pp. 57–91.

[15] N. P. Raju, J. E. Greedan, and M. A. Subramanian, Phys. Rev. B **49**, 1086 (1994); Y. Shimakawa, Y. Kubo, and T. Manako, Nature **379**, 53 (1996).

[16] L. Soderholm, C. V. Stager, and J. E. Greedan, J. Solid State Chem. **43**, 175 (1982); L. Soderholm, J. E. Greedan, and M. F. Collins, *ibid*. **35**, 385 (1980).

[17] J. A. Mydosh, *Spin Glasses* (Taylor & Francis, London, 1993), p. 66.

[18] G. V. Bazuev, O. V. Makaroa, and G. P. Sheveikin, Russ. J. Inorg. Chem. **28**, 1088 (1983).

[19] J. O. Thomson and J. R. Thomson, J. Phys. F **11**, 247 (1981); Y. Hattori, K. Fukamichi, K. Suzuki, H. Aruga-Katori, and T. Goto, J. Phys. Condens. Matter **7**, 4193 (1995).

[20] G. Ferey, R. De Pape, M. Leblanc, and J. Pannetier, Rev. Chim. Mineral. **23**, 474 (1986).

[21] P. R. Bevington, *Data Reduction and Error Analysis for the Physical Sciences* (McGraw-Hill, New York, 1969).

[22] J. S. Pedersen, D. Posselt, and K. Mortensen, J. Appl. Crystallogr. **23**, 321 (1990).

[23] J. J. Rhyne, IEEE Trans. Magn. **MAG-21**, 1990 (1985).

[24] M. Arai, Y. Ishikawa, N. Saito, and H. Takei, J. Phys. Soc. Jpn. **54**, 781 (1985).

[25] A. Aharony and E. Pytte, Phys. Rev. B **27**, 5872 (1983).

[26] M. L. Spano, J. J. Rhyne, S. J. Pickart, S. K. Hasanian, R. J. Gambino, and T. R. McGuire, J. Appl. Phys. **61**, 3638 (1987).

[27] J. J. Rhyne and G. E. Fish, J. Appl. Phys. **57**, 3407 (1985).